Accepted Manuscript

Novel pyrazolopyrimidines: Synthesis, *in vitro* cytotoxic activity and mechanistic investigation

Ghaneya S. Hassan, Doaa E. Abdel Rahman, Yassin M. Nissan, Esraa A. Abdelmajeed, Tamer M. Abdelghany

PII: S0223-5234(17)30525-1

DOI: 10.1016/j.ejmech.2017.07.003

Reference: EJMECH 9566

To appear in: *European Journal of Medicinal Chemistry*

Received Date: 28 May 2017

Revised Date: 30 June 2017

Accepted Date: 2 July 2017

Please cite this article as: G.S. Hassan, D.E. Abdel Rahman, Y.M. Nissan, E.A. Abdelmajeed, T.M. Abdelghany, Novel pyrazolopyrimidines: Synthesis, *in vitro* cytotoxic activity and mechanistic investigation, *European Journal of Medicinal Chemistry* (2017), doi: 10.1016/j.ejmech.2017.07.003.

Graphical abstract

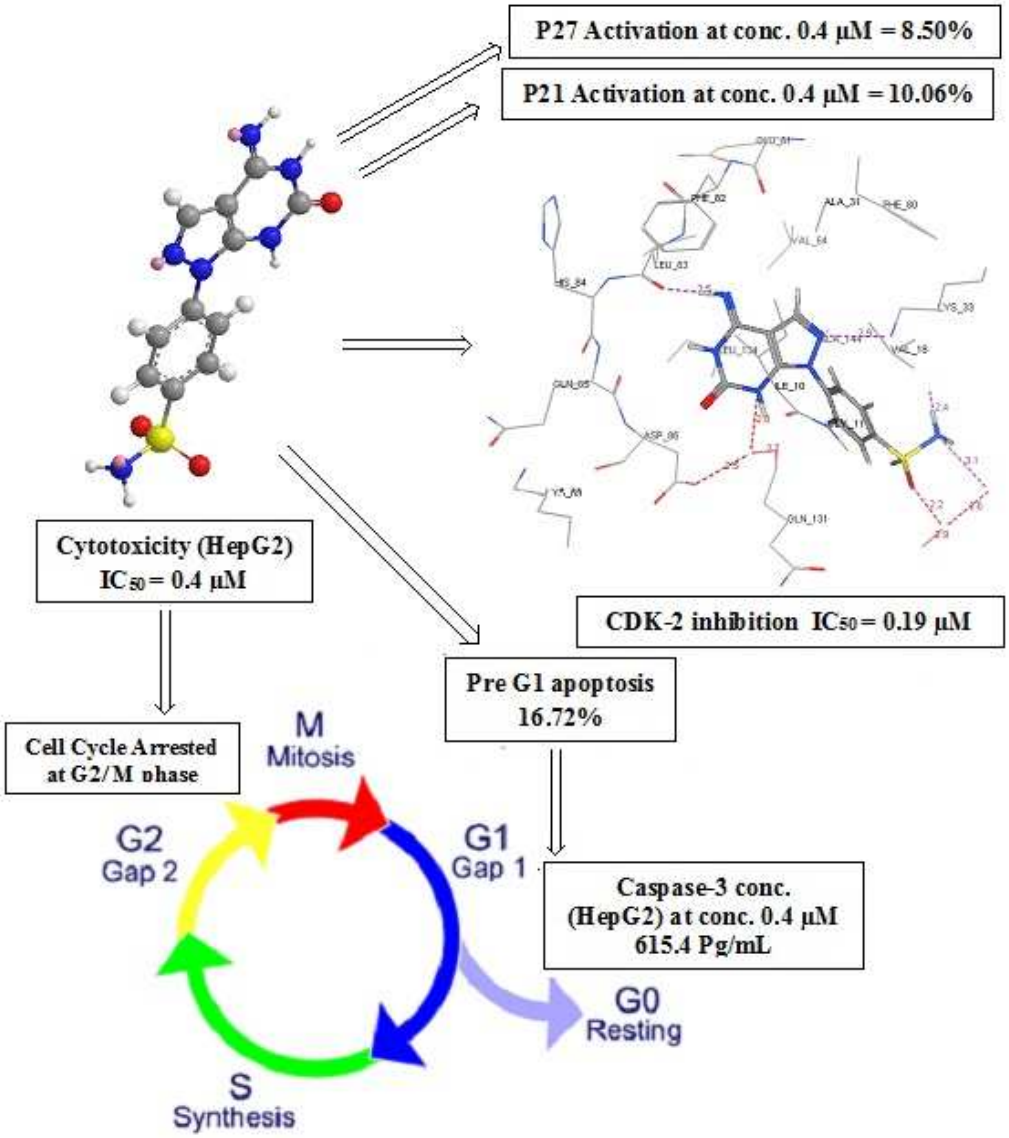

Novel pyrazolopyrimidines: Synthesis, *in vitro* cytotoxic activity and mechanistic investigation

Ghaneya S. Hassan[a], Doaa E. Abdel Rahman[a], Yassin M. Nissan[a*], Esraa A. Abdelmajeed[b] and Tamer M. Abdelghany[c].

[a]*Pharmaceutical Chemistry Department, Faculty of Pharmacy, Cairo University, Kasr Elini St., Cairo 11562, Egypt.*

[b]*National Cancer Institute, Cairo University, Fom Elkhalig, Kasr Elaini St., Cairo 11796, Egypt*

[c]*Pharmacology and Toxicology Department, Faculty of Pharmacy, Al-Azhar University, Nasr City, Cairo 11787, Egypt.*

**Corresponding author: Y. M. Nissan, Pharmaceutical Chemistry Department, Faculty of Pharmacy, Cairo University, Kasr Elini Street., Cairo 11562, Egypt.*

Tel.: +201000848844; E-mail address: yassin.nissan@hotmail.com

Abstract

A series of novel pyrazolo[3,4-*d*]pyrimidines bearing benzenesulfonamide moiety **5a-f, 6** and **7** were synthesized. Cytotoxic screening was conducted against MCF-7 and HepG2. 6-(4-Methoxyphenyl)-4-oxopyrazolopyrimidine derivative **5e** and 4-imino-6-oxopyrazolopyrimidine derivative **6** revealed potent cytotoxic activity with IC_{50} 1.4 µM (MCF-7) and 0.4 µM (HepG2), respectively compared to that of doxorubicin, (IC_{50} = 1.02 µM and 0.9 µM, respectively). Compounds **5e** and **6** were subjected to cell cycle analysis and apoptosis assay after 24h and 48h treatment. Compound **5e** arrested cell at G1 phase, while **6** arrested cell at S and G2/M phases, respectively. The apoptotic effect of both compounds were evidenced by pre G1 apoptosis as its percentage increased by time (7.38%, 11.61%) and (13.92%, 16.71%), respectively. Apoptosis induction capability was confirmed by the effect on early and late apoptosis and augmentation of caspase-3 level. Furthermore, compound **6** inhibited CDK2 enzyme with IC_{50} = 0.19 µM and increased levels of its regulators, P21 and P27 by 10.06% and 8.5%, respectively. Moreover, a molecular docking study of compound **6** on CDK2 enzyme was adopted to explore binding interaction with amino acid residues of its active site.

Key words: pyrazolopyrimidines; cytotoxicity; CDK2 inhibitor; apoptosis.

1. Introduction

Cancer, according to World Health Organization (WHO), is the second leading cause of death globally and accounted for 8.8 million deaths in 2015. That is nearly 1 in 6 of all global deaths [1]. Higher proliferation rate and evasion of apoptosis are considered two of common cancer hallmarks [2]. Cell division and programmed cell death "apoptosis" are intimately coupled [3]. The linkage of cell cycle and apoptosis has been influenced by some proteins like tumor protein (p53), Protein Kinase C (PKC), B-cell lymphoma 2 (Bcl-2), Nuclear Factor kappa-light-chain-enhancer of activated B cells (NF-κB), Cyclin Dependant Kinase (CDK), cyclins and Casein Kinase I (CKI) [4]. Cyclin dependent kinases (CDKs) are the master regulators that drive the cell cycle engine [5]. Their activities are down regulated by inhibitors (CDKIs) [6]. Deregulation of CDKs can activate CDKs inappropriately and as a consequence, promote proliferation of cancer [7]. CDK2, the S-phase CDK, control the G1/S transition. Also, regulate the G2/M transition that prevents cells with damaged DNA from initiating mitosis [8]. Also CDK2 participate in subset of apoptosis cascade [9]. Inhibition of CDK2 activity causes cell cycle arrest at G1/S and G2/M phases and induction of apoptosis [10]. Consequently, the development of CDK inhibitors might offer selective and tolerable treatment for cancer.

During the past decade many CDK inhibitors have been developed and characterized. The first CDK inhibitor, purine derivative, Roscovitine **I** is considered as a pan-selective CDK inhibitor with multiple effects on cell proliferation, cell cycle progression and induction of apoptosis in cancer cells [11]. However, Roscovitine exhibited toxicity and low efficacy [7]. Dinaciclib **II** is a pyrazolo[1,5-*a*]pyrimidine derivative that inhibits (CDKs). It is being evaluated in clinical trials for various cancer indications [12], (**Figure 1)**.

Literature survey revealed the biological activity of pyrazolo[3,4-*d*]pyrimidine, an isoster of purine, as CDK2 inhibitors and apoptotic inducers [7,11,13]. It was reported that, presence of benzenesulfonamide group on pyrazolo[3,4-*d*]pyrimidine scaffold strengthens its anticancer activity [14].

Inspired by the above findings, we aimed to design and synthesize CDK2 inhibitors with pyrazolo[3,4-*d*]pyrimidine scaffold bearing benzenesulfonamide moiety **5-7**. In order to explore the activity of the synthesized compounds, *in vitro* cytotoxic screening against liver cancer (HepG2) and breast cancer (MCF-7) cell lines was conducted. Moreover, to elucidate the mechanism of action for cytotoxic activity, the most active compounds were subjected to cell

cycle analysis and apoptotic assay. In addition, the CDK2 enzyme inhibition assay was conducted. Finally, simulation docking study was carried out to gain insight into the possible binding mode of the tested compound in the CDK2 enzyme binding site.

2. Results and Discussion

2.1. Chemistry

Sulfanilamide **1** was diazotized in hydrochloric acid with sodium nitrite at 5 °C. The diazonium salt was then reduced by sodium sulfite to give the 4-hydrazinobenzenesulfonamide **2** [15]. The key intermediate, 4-(5-amino-4-cyano-1*H*-pyrazol-1-yl)benzenesulfonamide **3** was prepared by reacting compound **2** with ethoxymethylene malononitrile in absolute ethanol and anhydrous sodium acetate [16]. The reaction proceeded via SN^2 mechanism in two steps leading to intramolecular pyrazole cyclization [17,18].

Pyrazole-4-carboxamide derivative **4** was prepared by stirring amino compound **3** with sulfuric acid for 16 h at room temperature. Its IR spectrum revealed presence of bands at 3460, 3452, 3344, 3278 and 3170 cm^{-1} which correspond to 3 NH_2 groups. Also a new band at 1662 cm^{-1} was attributed to C=O; in addition to disappearance of band at 2216 cm^{-1} for CN group. Mass spectrum showed its molecular ion peak at m/z 281.

Pyrazolo[3,4-*d*]pyrimidin-4-one derivatives **5a-f** were achieved by reacting pyrazole-4-carboxamide **4** with the appropriate aromatic aldehyde using DMF as a solvent in the presence of iodine as mild Lewis acid and oxidant. ^{1}H NMR spectra of compounds **5a-f** showed the appearance of singlet signal at δ: 12.57-12.79 ppm attributed to pyrimidine NH proton in addition to increased number of aromatic protons. Compound **5b** showed a triplet signal at δ: 7.44 ppm and a doublet of doublet signal at δ: 8.31 ppm assigned to H-3´,5´ and H-2´,6´ protons of *p*-fluoro substituted phenyl moiety, respectively. This was explained on the basis of proton coupling with fluorine atom [19]. ^{1}H NMR spectrum of compound **5e** showed singlet signal at δ: 3.87 ppm attributed to OCH_3 protons while that of compound **5f** had two singlet signals at δ: 3.87 and 3.91 ppm attributed to two OCH_3 protons. ^{13}C NMR spectrum of **5d** showed signals of aromatic carbons. Mass spectra of **5a-f** showed their molecular ion peaks (**Scheme 1**).

Fusion of 5-aminopyrazole-4-carbonitrile, **3** with urea yielded pyrazolopyrimidine derivative, **6**. IR spectrum of compound **6** showed the appearance of a band at 1685 cm^{-1} assigned to C=O group, while its ^{1}H NMR spectrum showed appearance of three singlet signals at δ: 7.48, 8.77

and 11.05 ppm attributed to three NH protons in addition to a singlet signal at δ: 7.37 ppm attributed to SO_2NH_2 protons. ^{13}C NMR spectrum of compound **6** showed signals corresponding to aromatic protons and mass spectrum showed its molecular ion peak at m/z 306.

4-(4-Amino-1*H*-pyrazolo[3,4-*d*]pyrimidin-1-yl)benzenesulfonamide **7** was achieved by refluxing amino derivative **3** with formamide for 16 h. ^1H NMR of compound **7** showed the appearance of the singlet signal at δ: 8.36 ppm which corresponds to H-3 pyrazolopyrimidine, and mass spectrum showed its molecular ion peak at m/z 290 (**Scheme 1**).

2.2. Biological Evaluation

2.2.1. Cytotoxic Screening

All newly synthesized compounds were tested against the human breast adenocarcinoma cell line (MCF-7), and human hepatocellular carcinoma cell line (HepG2) at the department of Pharmacology and Toxicology, Faculty of Pharmacy, Al-Azhar University by the method of MTT assay.

The newly synthesized compounds **3**, **4**, **5a-f**, **6** and **7** were evaluated for their *in vitro* cytotoxic activity against two cell lines using Doxorubicin as reference standard; all the results are displayed in **Table 1**.

Results showed that the synthesized pyrazole derivatives **3** and **4** were inactive against both MCF-7 and HepG2 cell lines, while the pyrazolo[3,4-*d*]pyrimidines **5-7** demonstrated variable activities against both cell lines. Substitutions at position 4 and 6 were proven crucial for pyrazolo[3,4-*d*]pyrimidines activity. 6-Substituted pyrazolo[3,4-*d*]pyrimidin-4-one derivatives with monosubstituted phenyl **5b-e** were very active, while unsubstituted **5a** and disubstituted **5f** were inactive against the both cell lines. Compound **5e** showed promising activity against MCF-7 with IC_{50} 1.40 µM comparable to the standard used doxorubicin with IC_{50} 1.02 µM, while it was inactive against HepG2. Also, compound **5c** showed good activity with IC_{50} 2.50 µM against MCF-7 and moderate activity with IC_{50} 23.90 µM against HepG2. Compound **5b** and **5d** exhibited mild activity against MCF-7 with IC_{50} 38 µM and 14.46 µM, respectively. However, against HepG2 compound **5b** showed good activity with IC_{50} 2.66 µM and compound **5d** showed mild activity with IC_{50} 42.6 µM. On the other hand, compound **6** showed promising activity against HepG2 cell line with IC_{50} 0.40 µM even more active than doxorubicin with IC_{50} 0.90 µM.

4-Substituted pyrazolo[3,4-*d*]pyrimidin-4-one with amino group, compound **7**, showed mild activity against MCF-7 with IC_{50} 40.70 µM.

Therefore, compounds **5e** and **6** were subjected to further investigations to explore the possible mechanism of action on MCF-7 and HepG2, respectively.

2.2.2. Cell cycle analysis and apoptosis assay

Compounds **5e** and **6** were subjected to cell cycle analysis, apoptotic assay and enzyme assays at confirmatory diagnostic unit, VACSERA-EGYPT.

2.2.2.1. Cell cycle analysis and apoptosis detection

Cell cycle is the series of growth and development steps that lead to cell division and DNA replication. The cell cycle consists of four distinct phases: G1 phase, S phase (synthesis), G2 phase and M phase. During G1, preparation of energy and DNA replication blocks occurs. The S phase is the stage when DNA replicates. During G2, the new DNA is checked and repaired. The M (mitosis) stage where nuclear and cytoplasmic division take place.

Effect of compounds **5e** and **6** on cell cycle progression and induction of apoptosis in the MCF-7 and HepG2 cell lines was studied. MCF7 and HepG2 cell lines were incubated with IC_{50} concentration of compound **5e** and **6** for 24 h and 48 h. The cell lines were stained with PI / Annexin V and analyzed by flow cytometry using BD FASCC alibur. Quantification of the results (**Table 2, Figure 2**) revealed that percentage of pre G1 apoptosis induced by compound **5e** on MCF-7 after 24h incubation was 7.38%. This percent was increased to 11.61% after 48h. A high percent of cell accumulation was observed in G1 and S phase in MCF-7 treated with compound **5e** after 24h and 48h incubation indicating arrest of cell cycle at G1/S transition. Compound **6** on HepG2 induced pre G1 apoptosis by 13.92% after 24h incubation that increased to 16.71% after 48h incubation. Also, HepG2 treated with compound **6** showed cell accumulation at S phase and G2/M phase after 24h incubation. It showed high cell accumulation at G2/M after 48h incubation. This indicated that it arrested cell cycle at G2/M phase.

2.2.2.2. Apoptosis assay

Cell cycle analysis of MCF-7 and HepG2 after treatment with compound **5e** and **6**, respectively showed presence of pre-G1 peak which is an indication of apoptosis. To confirm the ability of both compounds to induce apoptosis, cells were stained with Annexin V/ PI, incubated for 24h

and 48h and analyzed. Analyses of early and late apoptosis showed that, compounds **5e** and **6** were indeed able to induce significant levels of apoptosis (**Table 3, Figure 3**).

2.2.2.3. Caspase-3 activity (Key executor of apoptosis)

Caspases (cysteinyl aspartate specific proteinases) are essential in the regulation of apoptosis. There are two types of apoptotic caspases: Initiator (apical) caspases and effector (executioner) caspases. The best recognized biochemical hallmark of apoptosis is the activation of caspases. Detection of active caspase-3 in cells and tissues is an important method for apoptosis induced by a wide variety of apoptotic signals. Sensitive and reproducible detection of active caspase-3 is important to advance the understanding of cellular functions and multiple pathologies of etiologies [20,21]. Compounds **5e** and **6** were subjected to caspase-3 activation assay using ELISA technique. Results were expressed in term of Caspase-3 concentration Pg/ml (**Table 4**). From the table of the result, it was found that compound **5e** increased caspase-3 concentration in MCF-7 by 32 fold, while compound **6** induced activation caspase-3 in HepG2 by 36 fold compared to its control. In light of these results, both compounds may be considered as promising apoptotic inducers.

2.2.2.4. Cyclin dependent Kinase 2 (in vitro) inhibition assay (IC_{50} determination)

Cyclin-dependent kinases (CDKs) are a family of serine/threonine kinases where their catalytic activities are modulated by interactions with cyclins and Cdk inhibitors (CKIs). The regulation of the cell cycle is a well orchestrated pairing of different members of the cyclin dependent kinases (CDKs) and its regulatory subunits (cyclin). For instance, binding of CDK2 with cyclin E is necessary for cells to make the transition from G1 into S phase [8]. Association of CDK2 with cyclin A is responsible for DNA synthesis [9] and activation of M-cyclin/CDK complex [8].

The activity of CDKs is restrained by CDK inhibitors (CKIs). CKIs are subdivided into two classes based on their structure and CDK specificity. One of them are Cip/Kip family members [$p21^{Cip1}$ (Cdkn1a), $p27^{Kip1}$ (Cdkn1b) and $p57^{Kip2}$ (Cdkn1c)] are more promiscuous and interfere with the activities of cyclin E-, A- and B-dependent kinase complexes [5].

To elucidate the S phase and G_2/M phase arrest caused by compound **6**, the kinase inhibitory effect of **6** was evaluated against CDK2 and its IC_{50} was determined. After treatment with

different concentration of compound **6,** IC_{50} was calculated from concentration–response curve to be 0.19 µM (**Table 5**).

2.2.2.5. P21 and P27 expression

Compound **6** was subjected to P21 and P27 (CDKs inhibitors) expression assay to evaluate its effect on both. Results were expressed in term of residual concentration Pg/mL and % activation (**Table 6**). Compound **6** was found to activate P21 by 10.06% and P27 by 8.5% which will be reflected on CDK2 inhibition.

2.3. Molecular docking

CDK2 includes primarily the conserved kinase core with no extension at the N terminus and a short extension of 12 residues at the C terminus with small insert within the core. This catalytic core made up of ATP binding pocket, PSTAIRE-like cyclin-binding site and protein substrate binding site [22]. The backbone structure of CDK2 can be divided into two lobes. The smaller N-terminal lobe of CDK2 consists of a sheet of five antiparallel β-strands (β1-β5) and a single large helix (α1). The larger C-terminal lobe contains a pseudo-4-helical bundle (α2-α4, α6), a small β-ribbon (β6-β8) and two additional helices (α5, α7) [22]. CDK2 regulation, both positive and negative, depends on complexion with cyclins and its phosphorylation state. The ATP-binding pocket is a CDK2-Mg^{2+}ATP binary complex. Its site is found in the cleft between the two lobes [23]. Thr14 and Tyr15 are both in the middle of the glycine- rich loop that serves as a phosphate anchor in ATP binding. Also, it is considered as CDK2 inhibitory phosphorylation site. Thr160 is found at the apex of the T-loop, is considered as CDK2 activating phosphorylation site. The hydroxyl group of Thr160 is oriented toward the glycine rich loop of the ATP binding site.

The ATP phosphates are held in position by ionic and hydrogen bonding interactions with several residues including Lys33, Asp145 and the backbone amides of the glycine rich loop between β1 and β2. Oxygen from each of the three phosphates of ATP contributes to the octahedral co-ordination of the Mg^{2+} ion. The three other residues involved in the co-ordination of Mg^{2+} are Asn132, Asp145 and a water molecule [23].

In order to explore the binding mode of compound **6** on the active site of CDK2, molecular docking of compound **6** was performed using protein data bank file (PDB: 1y8y) [24] by

Molecular Operating Environment (MOE) 2008.10 release of Chemical Computing Group, Canada.

The binding affinity of the ligand was evaluated with energy score (S, Kcal/mol). Low dock score indicates good affinity. Hydrogen bond, arene arene and arene cation interaction were also used to assess the binding models.

The inhibitor CT7-CDK2 complex was precisely reproduced by the docking procedure as demonstrated by low root mean square deviation, rmsd (0.2341) and dock score (-18.0923 kcal/mol), i.e. the docking protocol was valid. As shown in (**Figure 4)** the inhibitor CT7 (IC_{50} = 2.0 µM) [24] nearly fits in the active site forming eight hydrogen bonding interactions with the active site residues. N of pyrimidine binds with Lys33 (3.17 Å). Leu83 interacts by two hydrogen bonds with NH (2.70 Å) and N pyrazole (3.10 Å). SO_2 of ligand interacts with Asp86 (2.90 Å) and Lys89 (3.18 Å) and also through water molecule with His84, Gln85 and Lys89 (3.11 Å).

Compound **6** (IC_{50} 0.19 µM) with dock score (-18.6608 Kcal/mol), binds with active site forming eight hydrogen bonds in addition to one arene cation interaction. The amino group of SO_2NH_2 binds with Thr14 (2.55 Å) and Asp145 (1.29 Å). N of pyrazole interacts with Lys33 (2.93 Å) and the imino NH interacts with Leu83 (2.50 Å). In addition, the oxygen atom of SO_2NH_2 binds with Thr14 and Lys123 through water molecule (2.24 Å) while NH of pyrimidine binds with Asp86 and Gln131 through water molecule (1.94 Å) in addition to arene cation interaction between benzene ring and Lys33, reflecting its action as CDK-2 inhibitor (**Figure 5**).

3. Conclusion

In this study, a series of pyrazolopyrimidine derivatives were synthesized and their cytotoxicity against MCF-7 and HepG2 were evaluated. It was found that; compound **5e** was potent against MCF-7 with IC_{50} comparable to standard used (Doxorubicin). However, pyrazolopyrimidine **6** demonstrated high potency against HepG2 with IC_{50} less than standard used doxorubicin. Moreover, the potential mechanisms of the cytotoxic activity of the promising compounds **5e** and **6** on MCF-7 and HepG2 cell lines were investigated. Cell cycle analysis showed that pyrazolopyrimidine derivative **5e** arrested cell cycle of MCF-7 at G1 phase. While pyrazolopyrimidine derivative **6** arrested cell cycle of HepG2 at S and G2/M phases. Also, both

compounds exhibited apoptotic induction capability. This was evidenced by presence of pre G1 peak and confirmed by apoptotic induction assay and augmenting caspase-3 activation. In the light of cell cycle results, compound **6** subjected to CDK2 inhibition assay with IC_{50} 0.19 µM. Furthermore, it increased the expression of CDK2 inhibitors P21 and P27. Molecular docking of compound **6** on CDK2 enzyme (PDB: 1y8y) confirmed the biological results.

4. Experimental

4.1. Chemistry

Melting points were determined on Stuart melting point apparatus (Stuart Scientific, Redhil, UK) and Peak Find-Memory-9 and were uncorrected. IR spectra were recorded as potassium bromide disc on Shimadzu FT-IR Affinity-1 spectrometer and Bruker FT-IR spectrophotometer. They were expressed in wave number (cm^{-1}). The NMR spectra were recorded on a Varian Mercury VX-300 and Bruker AVANCE III400 MHz FT-NMR spectrometer. ^1H spectra were run at 400 MHz and ^{13}C spectra were run at 100 MHz in deuterated dimethylsulphoxide (DMSO-d_6). Chemical Shifts are quoted in δ as parts per million (ppm) downfield from tetramethylsilane (TMS) as internal standard. Mass spectra were recorded using Single Quadruple mass spectrometer ISQ LT. Microanalyses were carried out at The Regional Center for Mycology and Biotechnology, Al-Azhar University. TLC were carried out using Kieselgel 60 F254 sheets (Merck, Darmstadt, Germany), the developing solvents were dichloromethane/methanol (9:1) and the spots were visualized at 366, 254 nm by UV Vilber Lourmat 77202 (Vilber, Marne La Vallee, France).

4-Hydrazinobenzenesulfonamide HCl, **2** [15] and 4-(5-amino-4-cyano-1*H*-pyrazol-1-yl)benzenesulfonamide **3** [16] were synthesized according to the reported methods.

4.1.1. *5-Amino-1-(4-sulfamoylphenyl)-1H-pyrazole-4-carboxamide* **4**

The 5-aminopyrazole-4-carbonitrile **3** (0.26 g, 1 mmol) was stirred in sulfuric acid (8.2 mL) at room temperature for 16 h. The reaction mixture was poured on crushed ice (50 mL) and was neutralized with saturated sodium bicarbonate solution. The crude solid was filtered, washed with water, dried and crystallized from ethanol.

R_f=0.12; yield: 88%; mp 161 °C (decomp.); ^1H NMR (400 MHz, DMSO-d_6) δ ppm: 6.58 (s, 2H, NH_2, exch. D_2O), 7.50 (s, 2H, SO_2NH_2 exch. D_2O), 7.78 (d, J = 8.7 Hz, 2H, H-2,6 Ar), 7.94 (d, J

= 8.6 Hz, 3H, H-3 pyrazole, H-3,5 Ar), 7.97 (s, 2H, $CONH_2$, exch. D_2O); IR (KBr) υ_{max}\cm^{-1}: 3460, 3452, 3344, 3278, 3170 ($3NH_2$), 3076 (CH Ar), 1662 (C=O), 1612, 1593, 1566, 1543 (C=N, NH, C=C), 1327, 1168 (SO_2); MS (70 eV): m/z (%): 281 (3.53) [M^+]; elemental analysis calcd (%) for $C_{10}H_{11}N_5O_3S$: C 42.70, H 3.94, N 24.90; Found: C 42.94, H 3.75, N 25.12.

4.1.2. *General Procedure for synthesis of compounds* **5a-f**

A mixture of compound **4** (0.28 g, 1 mmol), appropriate aromatic aldehyde (1 mmol) and molecular iodine (0.285 g, 2 mmol) was heated at 80 °C in dimethylformamide (5 mL) for 12-16 h (reaction monitored by TLC). The reaction mixture was cooled, poured on crushed ice and aqueous solution of 5% sodium thiosulfate (15 mL) was added. The precipitate was filtered, washed and dried. The crude product was crystallized from methanol.

4.1.2.1.*4-(4-Oxo-6-phenyl-4,5-dihydro-1H-pyrazolo[3,4-d]pyrimidin-1-yl)benzenesulfonamide* **5a**

Reaction time 16 h; R_f=0.45; yield: 80 %; mp 250 °C (decomp.); ^{1}H NMR (400 MHz, DMSO-d_6) δ ppm: 7.47 (s, 2H, SO_2NH_2 exch. D_2O), 7.59 (t, *J* = 7.6 Hz, 2H, H-3´,5´Ar), 7.65 (d, *J* = 7.3 Hz, 1H, H-4´Ar), 8.05 (d, *J* = 8.5 Hz, 2H, H-2,6 Ar), 8.23 (d, *J* = 7.3 Hz, 2H, H-2´,6´ Ar), 8.40 (d, *J* = 8.7 Hz, 2H, H-3,5 Ar), 8.44 (s, 1H, H-3 pyrazolopyrimidine), 12.74 (s, 1H, NH exch. D_2O); IR (KBr) υ_{max}\cm^{-1}: 3363, 3240, 3178 (NH_2, NH), 3066 (CH Ar), 1670 (C=O), 1624, 1600, 1550, 1523, 1500 (C=N, NH, C=C), 1346, 1157 (SO_2); MS (70 eV): m/z (%): 367 (54.90) [M^+]; elemental analysis calcd (%) for $C_{17}H_{13}N_5O_3S$: C 55.58, H 3.57, N 19.06; Found: C 55.83, H 3.63, N 19.42.

4.1.2.2.*4-[6-(4-Fluorophenyl)-4-oxo-4,5-dihydro-1H-pyrazolo[3,4-d]pyrimidin-1-yl] benzenesulfonamide* **5b**

Reaction time 16 h; R_f=0.47; yield: 75%; mp >300 °C; ^{1}H NMR (400 MHz, DMSO-d_6) δ ppm: 7.44 (t, *J* = 8.8 Hz, 2H, H-3´,5´Ar), 7.47 (s, 2H, SO_2NH_2 exch. D_2O), 8.04 (d, *J* = 8.7 Hz, 2H, H-2,6 Ar), 8.31 (dd, *J* = 8.7, 5.4 Hz, 2H, H-2´,6´Ar), 8.39 (d, *J* = 8.7 Hz, 2H, H-3,5 Ar), 8.43 (s, 1H, H-3 pyrazolopyrimidine), 12.76 (s, 1H, NH exch. D_2O); IR (KBr) υ_{max}\cm^{-1}: 3367, 3240, 3209 (NH_2, NH), 3089 (CH Ar), 1662 (C=O), 1600, 1597, 1558, 1527 (C=N, NH, C=C), 1350, 1165 (SO_2); MS (70 eV): m/z (%): 385 (1.41) [M^+]; elemental analysis calcd (%) for $C_{17}H_{12}FN_5O_3S$: C 52.98, H 3.14, N 18.17; Found: C 53.17, H 3.26, N 18.43.

4.1.2.3.*4-[6-(4-Chlorophenyl)-4-oxo-4,5-dihydro-1H-pyrazolo[3,4-d]pyrimidin-1-yl]benzenesulfonamide* **5c**

Reaction time 12 h; R_f=0.64; yield: 80%; mp >300 °C; ^{1}H NMR (400 MHz, DMSO-d_6) δ ppm: 7.47 (s, 2H, SO_2NH_2 exch. D_2O), 7.66 (d, *J* = 8.5 Hz, 2H, H-3´,5´Ar), 8.04 (d, *J* = 8.7 Hz, 2H, H-2,6 Ar), 8.24 (d, *J* = 8.6 Hz, 2H, H-2´,6´ Ar), 8.38 (d, *J* = 8.7 Hz, 2H, H-3,5 Ar), 8.43 (s, 1H, H-3 pyrazolopyrimidine), 12.76 (s, 1H, NH exch. D_2O); IR (KBr) υ_{max}\cm^{-1}: 3325, 3224, 3167 (NH_2, NH), 3080 (CH Ar), 1693 (C=O), 1612, 1597, 1543 (C=N, NH, C=C), 1346, 1161 (SO_2); MS (70 eV): m/z (%): 401 (0.79) [M^+]; elemental analysis calcd (%) for $C_{17}H_{12}ClN_5O_3S$: C 50.81, H 3.01, N 17.43; Found: C 51.12, H 3.04, N 17.78.

4.1.2.4.*4-[6-(4-Bromophenyl)-4-oxo-4,5-dihydro-1H-pyrazolo[3,4-d]pyrimidin-1-yl]benzenesulfonamide* **5d**

Reaction time 12 h; R_f=0.51; yield: 80%; mp >300 °C; ^{1}H NMR (400 MHz, DMSO-d_6) δ ppm: 7.48 (s, 2H, SO_2NH_2 exch. D_2O), 7.79 (d, *J* = 8.4 Hz, 2H, H-3´,5´Ar), 8.04 (d, *J* = 8.7 Hz, 2H, H-2,6 Ar), 8.15 (d, *J* = 8.6 Hz, 2H, H-2´,6´ Ar), 8.38 (d, *J*=8.7 Hz, 2H, H-3,5 Ar), 8.43 (s, 1H, H-3 pyrazolopyrimidine), 12.79 (s, 1H, NH exch. D_2O); ^{13}C NMR (100 MHz, DMSO-d_6) δ ppm: 106.94 (C3a pyrazolopyrimidine), 121.94 (C3,5), 126.58 (C4´), 127.53 (C2,6), 130.85 (C3´,5´), 131.53 (C1´), 132.28 (C2´,6´), 137.38 (C1), 141.10 (C4), 142.50 (C3 pyrazolopyrimidine), 153.12 (C7a pyrazolopyrimidine), 156.09 (C6 pyrazolopyrimidine), 158.50 (C4 pyrazolopyrimidine); IR (KBr) υ_{max}\cm^{-1}: 3332, 3232, 3167 (NH_2, NH), 3109 (CH Ar), 1693 (C=O), 1600, 1590, 1543, 1500 (C=N, NH, C=C), 1346, 1161 (SO_2); MS (70 eV): m/z (%): 446 (0.95) [M^+], 448 (1.60) [M^++2]; elemental analysis calcd (%) for $C_{17}H_{12}BrN_5O_3S$: C 45.75, H 2.71, N 15.69; Found: C 46.02, H 2.74, N 15.87.

4.1.2.5.*4-[6-(4-Methoxyphenyl)-4-oxo-4,5-dihydro-1H-pyrazolo[3,4-d]pyrimidin-1-yl]benzenesulfonamide* **5e**

Reaction time 16 h; R_f=0.49; yield: 80%; mp >300 °C; ^{1}H NMR (400 MHz, DMSO-d_6) δ ppm: 3.87 (s, 3H, OCH_3), 7.13 (d, *J* = 8.8 Hz, 2H, H-3´,5´Ar), 7.46 (s, 2H, SO_2NH_2 exch. D_2O), 8.04 (d, *J* = 8.7 Hz, 2H, H-2,6 Ar), 8.24 (d, *J* = 8.4 Hz, 2H, H-2´,6´ Ar), 8.40 (d, *J* = 8.6 Hz, 3H, H-3 pyrazolopyrimidine, H-3,5 Ar), 12.57 (s, 1H, NH exch. D_2O); IR (KBr) υ_{max}\cm^{-1}: 3356, 3244, 3197 (NH_2, NH), 3028 (CH Ar), 1685 (C=O), 1612, 1593, 1558 (C=N, NH, C=C), 1330, 1157 (SO_2); MS (70 eV): m/z (%): 397 (4.58) [M^+]; elemental analysis calcd (%) for $C_{18}H_{15}N_5O_4S$: C 54.40, H 3.80, N 17.62; Found: C 54.69, H 4.06, N 17.27.

4.1.2.6.*4-[6-(3,4-Dimethoxyphenyl)-4-oxo-4,5-dihydro-1H-pyrazolo[3,4-d]pyrimidin-1-yl]benzenesulfonamide* **5f**

Reaction time 16 h; R_f=0.46; yield: 80%; mp 263 °C (decomp.); ^{1}H NMR (400 MHz, DMSO-d_6) δ ppm: 3.87 (s, 3H, OCH_3), 3.91 (s, 3H, OCH_3), 7.17 (d, *J* = 8.5 Hz, 1H, H-5´Ar), 7.47 (s, 2H, SO_2NH_2 exch. D_2O), 7.85 (s, 1H, H-2´Ar), 7.94 (d, *J* = 8.5 Hz, 1H, H-6´Ar), 8.04 (d, *J* = 8.7 Hz, 2H, H-2,6 Ar), 8.41 (s, 1H, H-3 pyrazolopyrimidine), 8.43 (d, *J* = 8.7 Hz, 2H, H-3,5 Ar), 12.57 (s,1H, NH exch. D_2O); IR (KBr) υ_{max}\cm^{-1}: 3356, 3259, 3201 (NH_2, NH), 3093 (CH Ar), 1685 (C=O), 1600, 1597, 1560, 1531 (C=N, NH, C=C), 1342, 1161 (SO_2); MS (70 eV): m/z (%): 427 (1.18) [M^+]; elemental analysis calcd (%) for $C_{19}H_{17}N_5O_5S$: C 53.39, H 4.01, N 16.38; Found: C 53.69, H 4.06, N 16.42.

4.1.3.*4-(4-Imino-6-oxo-4,5,6,7-tetrahydro-1H-pyrazolo[3,4-d]pyrimidin-1-yl)benzenesulfonamide* **6**

A mixture of aminocyanopyrazole compound **3** (0.55 g, 2 mmol) and urea (0.5 g, 8 mmol) was heated at 200 °C for 20 min. (till the melted solution became a solid mass). The reaction mixture was cooled and the yellowish brown precipitate was solubilized in 2N sodium hydroxide and heated till boil (clear solution) then acidified with dilute hydrochloric acid. The obtained solid, re-precipitated twice, was filtered, washed with water and dried. The crude product was crystallized from ethanol.

R_f=0.2; yield: 88%; mp >300 °C; ^{1}H NMR (400 MHz, DMSO-d_6) δ ppm: 7.37 (s, 2H, SO_2NH_2 exch. D_2O), 7.48 (s, 1H, NH exch. D_2O), 7.92 (d, *J* = 8.7 Hz, 2H, H-2,6 Ar), 8.21 (s, 1H, H-3 pyrazolopyrimidine), 8.41 (d, *J* = 8.7 Hz, 2H, H-3,5 Ar), 8.77 (s, 1H, NH exch. D_2O), 11.05 (s, 1H, NH exch. D_2O); ^{13}C NMR (100 MHz, DMSO-d_6) δ ppm: 93.22 (C3a pyrazolopyrimidine), 119.97 (C3,5), 127.16 (C2,6), 136.98 (C7a pyrazolopyrimidine), 140.71 (C1), 142.15 (C3 pyrazolopyrimidine), 153.97 (C4), 156.83 (C4 pyrazolopyrimidine), 159.12 (C6 pyrazolopyrimidine); IR (KBr) υ_{max}\cm^{-1}: 3402, 3317 (NH_2, 3NH), 3086 (CH Ar), 1685 (C=O), 1612, 1593, 1563, 1516 (C=N, NH, C=C), 1307, 1153 (SO_2); MS (70 eV): m/z (%): 306 (1.46) [M^+]; elemental analysis calcd (%) for $C_{11}H_{10}N_6O_3S$: C 43.13, H 3.29, N 27.44; Found: C 43.28, H 3.40, N 27.78.

4.1.4. *4-(4-Amino-1H-pyrazolo[3,4-d]pyrimidin-1-yl)benzenesulfonamide* **7**

A mixture of compound **3** (0.55 g, 2 mmol) and formamide (3 mmol) was heated under reflux for 16 h. The reaction mixture was cool, poured onto ice-water, filtered and dried. The crude product was crystallized from methanol.

R_f=0.38; yield: 88%; mp >300°C; ^{1}H NMR (400 MHz, DMSO-d_6) δ ppm: 7.42 (s, 4H, NH_2, SO_2 NH_2 exch. D_2O), 7.99 (d, *J* = 8.0 Hz, 2H, H-2,6 Ar), 8.36 (s, 1H, H-6 pyrazolopyrimidine), 8.43 (s, 1H, H-3 pyrazolopyrimidine), 8.47 (d, *J* = 8.0 Hz, 2H, H-3,5 Ar); IR (KBr) υ_{max}\cm^{-1}: 3414, 3398, 3242, ($2NH_2$), 3080 (CH Ar), 1660, 1587, 1562, 1504 (C=N, NH, C=C), 1327, 1155 (SO_2); MS (70 eV): m/z (%): 290 (9.03) [M^+]; elemental analysis calcd (%) for $C_{11}H_{10}N_6O_2S$: C 45.51, H 3.47, N 28.95. Found: C 45.67, H 3.14, N 29.15.

4.2. Biological Evaluation

4.2.1. Cytotoxicity screening

Exponentially growing cells from two cancer cell lines were trypsinized, counted and seeded at the appropriate densities (2000-1000 cells/0.33 cm^2 well) into 96-well microtiter plates. Cells then were incubated in a humidified atmosphere at 37 ˚C for 24 h. Then, cells were exposed to different concentrations of compounds (0.1, 10, 100, 1000 µM) for 72 h. Then the viability of treated cells were determined using MTT technique as follow. Media were removed; cells were incubated with 200 µL of 5% MTT solution/well (Sigma Aldrich, MO) and were allowed to metabolize the dye into colored-insoluble formazan crystals for 2 h. The remaining MTT solution were discarded from the wells and the formazan crystals were dissolved in 200 µL/well acidified isopropanol for 30 min., covered with aluminum foil and with continuous shaking using a MaxQ 2000 plate shaker (Thermo Fisher Scientific Inc, MI) at room temperature. Absorbance was measured at 570 nm using a Stat FaxR 4200 plate reader (Awareness Technology, Inc., FL). The cell viability were expressed as percentage of control and the concentration that induces 50% of maximum inhibition of cell proliferation (IC_{50}) were determined using Graph Pad Prism version 5 software (Graph Pad software Inc, CA) [25,26].

4.2.2.1. Cell cycle analysis and apoptosis detection

The MCF-7 and HepG2 cell lines were treated with 1.4 µM of compound **5e** and 0.4 µM of compound **6**, respectively for 24 or 48 h. After treatment, the cells were suspended in 0.5 mL of PBS, collected by centrifugation, and fixed in ice-cold 70% (v/v) ethanol washed with PBS, re-suspended with 0.1 mg/mL RNase, stained with 40 mg/ml PI, and analyzed by flow cytometry using FACScalibur (Becton Dickinson). The cell cycle distributions were calculated using Phoenix Flow Systems and Verity Software House [27].

4.2.2.2. Apoptosis Assay

The MCF-7 and HepG2 were treated with 1.4 μ M of compound **5e** and 0.4 μM of compound **6** respectively for 24 or 48 h. After treatment, the cells were suspended in 0.5 mL of PBS, collected by centrifugation, and fixed in ice-cold 70% (v/v) ethanol, centrifuged the ethanol-suspended cells for 5 min, suspended in 5 mL PBS and centrifuged for 5 min., re-suspended with 1 mL PI staining solution (0.1 mg/ml RNase) + PE Annexin V (component no. 51-65875X) and kept in dark at 37 °C for 10 min., finally analyzed by flow cytometry using FACScalibur (Becton Dickinson). The cell cycle distributions were calculated using Phoenix Flow Systems and Verity Software House [28].

4.2.2.3. Caspase-3 activity (Key executor of apoptosis)

The Invitrogen Caspase-3 (active) Human ELISA is designed to detect and quantify the level of human active caspase-3 protein when cleaved at Asp175/Ser176. Briefly, MCF-7 and HepG2 cells were treated with **5e** (1.4 μM) and **6** (0.4 μM). The cells were harvested by trypsinization and rinsed with PBS. After centrifugation, the pellet (105- 106 cells) was suspended in 1 mL of PBS. Cells were freezed at < -20 ^{o}C and thawed with gentle mixing. Freeze/thaw cycle repeated for 3 times, then centrifuged at 1500×g for 10 min. at 2-8^{o}C to remove cellular debris. Human eia kit is a solid phase sandwich Enzyme Linked Immuno-Sorbent Assay (ELISA). A monoclonal specific antibody for human target protein has been coated onto the wells of the microtiter strips provided. Samples, including a standard containing the human target protein control specimens, and unknowns, are pipette into these wells and then a rabbit antibody specific for human active target protein is added to the wells. During the first incubation, the human target protein binds to the immobilized (capture) antibody and the specific active protein antibody serves as a detection antibody by binding to the immobilized active protein. After the first incubation step and washing to remove excess protein and detection antibody, a horseradish peroxidase-labeled Anti-Rabbit IgG (Anti-Rabbit IgG HRP) is added. This binds to the detection antibody to complete the four-member sandwich. After a third incubation and washing to remove all the excess Anti-Rabbit IgG HRP, a substrate solution is added, which is acted upon by the bound enzyme to produce color. The color intensity is measured using ROBONIK P2000 SPECTROPHOTOMETER at a wavelength of 450 nm. The intensity of this colored product is

directly proportional to the concentration of human active protein present in the original specimen [29].

4.2.2.4. Cyclin dependent Kinase 2 in vitro inhibition assay

This assay employs the quantitative sandwich enzyme immunoassay technique. Antibody specific for CDKN2A has been pre-coated onto a microplate. Standards and samples are pipette into the wells and any CDKN2A present is bound by the immobilized antibody. After removing any unbound substances, a biotin-conjugated antibody specific for CDKN2A is added to the wells. After washing, avidin conjugated horseradish peroxidase (HRP) is added to the wells. Following a wash to remove any unbound avidin-enzyme reagent, a substrate solution is added to the wells and color develops in proportion to the amount of CDKN2A bound in the initial step. The color development is stopped and the intensity of the color is measured using ROBONIK P2000 SPECTROPHOTOMETER at a wavelength of 450 nm. To determine IC_{50} different concentrations of compound **6** (0.004, 0.02, 0.1, 0.4 and 0.5 ug/mL) was performed. The IC_{50} value was calculated according to the equation for Boltzman sigmoidal concentration–response curve using the nonlinear regression fitting models (Graph Pad, Prism Version 5).

4.2.2.5. P21 and P27 expression

This assay employs the quantitative sandwich enzyme immunoassay technique. The kit used for $P21^{Cip1}$ is ab136945 –p21 Human ELISA kit while that used for $P27^{Kip1}$**DRG® Human p27 ELISA (EIA-4491)**. Samples and standards are added to wells coated with a monoclonal antibody specific for $P27^{Kip1}$. The plate is then incubated, washed, leaving only bound $p27^{Kip1}$ the plate. A yellow solution of polyclonal antibody to humanp27Kip1 is then added. This binds the p27Kip1 captured on the plate. The plate is then incubated, washed to remove excess antibody. A blue solution of HRP conjugate is added to each well, binding to the p27Kip1 polyclonal. The plate is again incubated, washed to remove excess HRP conjugate. TMB Substrate solution is added. The substrate generates a blue color when catalyzed by the HRP. Stop solution is added to stop the substrate reaction. The resulting yellow color intensity is measured using ROBONIK P2000 SPECTROPHOTOMETER at a wavelength of 450 nm.

*Same procedure is applied for $P21^{Cip}$

4.3. Molecular Docking

Docking study of the synthesized compound was performed by Molecular Operating Environment (MOE) 2008.10 release of Chemical Computing Group, Canada. The program operated under "Window XP" operating system installed on an Intel Pentium IV PC with a 2.8 MHz processor and 512 RAM. All minimizations were performed with MOE until a RMSD gradient of 0.05 Kcal mol^{-1} $Å^{-1}$ with MMFF94 force field and the partial charges were automatically calculated. The score function, dock function (S, Kcal/mol) developed by MOE program was used for the evaluation of the binding affinity of the ligand. The X-ray crystal structure of the enzyme (PDB code: 1y8y) [24] was obtained from the protein data bank in PDB format. The enzyme was prepared for docking studies: i) 3D protonation for the amino acid side chain and ligand. ii) Isolation of the active site, fixation to be dealt with as rigid structure and recognition of the amino acids. iii) Creation of dummies around the active site. iv) Studying the interaction of the ligand with the amino acids of the active site.

The 3D structure of the synthesized compound were built using MOE and subjected to the following procedure: i) 3D protonation of the structure. ii) Running conformational analysis using systemic search. iii) Selecting the least energetic conformer. iv) Applying the same docking protocol used with ligand.

Prior to the docking of the pyrazolopyrimidine derivative **6**, redocking of the native ligand bound in the CDK2 active site was performed to validate the docking protocol. The generated most stable conformer of the compound was virtually docked into the predefined active site of the CDK2. The developed docked models were energetically minimized and then used to predict the interaction of the ligand with the amino acids in the active site of the enzyme.

Acknowledgment

Authors thank Dr. Essam Rashwan, Head of confirmatory diagnostic unit, VACSERA-EGYPT for carrying out the cell cycle analysis, apoptosis and enzyme assays.

References

[1] Cancer Trends Progress Report. January 2017. WHO Website: http://www.who.int/cancer/en and http://progressreport.cancer.gov.

[2] Y. Lazebnik, *Nat. Rev. Cancer* **2010**, *10 (4),* 232-233.

[3] F. Q. Alenzi, *Br. J. Biomed. Sci.* **2004**, *61(2)*, 99-102.

[4] K. Vermeulen, Z. N. Berneman, D. R. VanBockstaele, *Cell Prolif.* **2003**, *36*, 165–175.

[5] S. Lim, P. Kaldis, *Develop.* **2013**, *140*, 3079-3093.

[6] A. Besson, S. F. Dowdy, J. M. Roberts, *Dev. Cell.* **2008**, *14 (2)*, 159-169.

[7] L. Vymětalová, L. Havlíček, A. Šturc, Z. Skrášková, R. Jorda, T. Pospíšil, M. Strnad, V. Kryštf, *Eur. J. Med. Chem.* **2016**, *110*, 291-301.

[8] J. H. Chung, F. Bunz, *PLoSGenet.* **2010**, *62*, e1000863.

[9] G. Gil-Gómez, *Methods Mol. Biol.* **2004**, *282*, 131-144.

[10] D. Guardavaccaro, M. Pagano, *Mol. Cell.* **2006**, *22(1)*, 1-4.

[11] R. Jorda, L. Havlícek, I. W. McNae, M. D Walkinshaw, J. Voller, A. Sturc, J. Navrátilová, M. Kuzma, M. Mistrík, J. Bártek, M. Strnad, V. Krystof, *J. Med. Chem.* **2011**, *54 (8)*, 2980-2993.

[12] A. J. Johnson, Y. Y. Yeh, L. L. Smith, A. J. Wagner, J. Hessler, S. Gupta, J. Flynn, J. Jones, X. Zhang, R. Bannerji, M. R. Grever, J. C. Byrd, *Leukemia* **2012**, *26 (12)*, 2554-2557.

[13] D. A. Ibrahim, A. M. El-Metwally, E. E. Al-Arab, *Arkivoc* **2009**, *7*, 12-25.

[14] H. M. A. Ashour, A. E. Abdel Wahab, *Arch. Pharm. Chem. Life Sci*. **2009**, *342*, 238- 252.

[15] M. Husnberger, E. R. Shak, J. Fugger, R. Ketcham, D. Lednicer, *Ber.* **1956**, *21*, 394-399.

[16] V. J. Ram, H. N. Pandey, *Arch. Pharm.* **1979**, *312*, 703-707.

[17] M. S. Al-Said, M. M. Ghorab, S. I. Al-qasoumi, E. M. El-Hossary, N. Noaman, *Eur. J. Med. Chem.* **2010**, *45(7)*, 3011-3018.

[18] M. M. Ghorab, F. A. Ragab, H. L. Heiba, R. M. El-Hazek, *Eur. J. Med. Chem.* **2011**, *46*, 5120-5126.

[19] R. M. Silverstein, F. X. Webster, D. G. Kiemle, Spectrophotometric identification of organic compounds. 7th ed., John Wiley and Sons. **2005**, pp.155.

[20] K. M. Boatright, G. S. Salvesen, *Curr. Opin. Cell Biol*. **2003**, *15*, 725-731.

[21] G. Cohen, *Biochem. J*. **1997**, *326*, 1-16.

[22] H. L. DeBondt, J. Rosenbiatt, J. Hancank, H. D. Jones, D. O. Morgan, S. H. Kim, *Nature* **1993**, *363*, 595- 602.

[23] E. Radzio-Andzelm, J. Lew, S. Taylor, *Structure* **1995**, *3 (11)*, 1135-1141.

[24] D. S. Williamson, M. J. Parratt, J. F. Bower, J. D. Moore, C. M. Richardson, P. Dokurno, A. D. Cansfield, G. L. Francis, R. J. Hebdon, R. Howes, P. S. Jackson, A. M. Lockie, J. B. Murray,

C. L. Nunns, J. Powles, A. Robertson, A. E. Surgenor, C. J. Torrance, *Bioorg. Med. Chem. Lett.* **2005**, *15 (4)*, 863–867.

[25] T. Mosmann, *J. Immunol. Methods* **1983**, *65*, 55-63.

[26] D. A. Scudiero, R. H. Shoemaker, D. K. Paull, A. Monks, S. Tierney, H. T. Nofziger, J. M. Currens, D. Seniff, M. R. Boyd, *Cancer Res.* **1988**, *48*, 4827-4833.

[27] I. Nicoletti, G. Migliorati, M. C. Pagliacci, F. Grignani, C. Riccardi, *J. Immunol. Methods* **1991**, *139*, 271-279.

[28] I. Vermes, C. Haanen, H. Steffens Nakken, C. P. Reutelingsperger, *J. Immunol. Methods* **1995**, *184*, 39-51.

[29] M. Andersson, J. Sjöstrand, A. Petersen, A. K. S. Honarvar, J. O. Karlsson, *Invest. Ophthalmol. Vis. Sci*. **2000**, *41 (9)*, 2623-2632.

Figures Captions

Figure 1: Chemical structure of some CDK2 inhibitors.

Figure 2: Cell cycle analysis of compound **5e** and **6** on MCF-7 and HepG2, respectively.

Figure 3: Apoptosis induction analysis using Annexin V/PI of compound **5e** and **6** on MCF-7 and HepG2, respectively.

Figure 4: 2D (above) and 3D (below) interaction of ligand CT7 on the active site of CDK2.

Figure 5: 2D (above) and 3D (below) interaction of compound **6** on the active site of CDK2.

Table 1: *In vitro* cytotoxic activity (IC_{50} µM) of compounds **3-7** against breast cancer cell line (MCF-7) and liver cancer cell line (HepG2).

Table 2: Cell Cycle analysis results for compounds **5e** and **6**.

Table 3: Apoptosis induction analysis using Annexin V/PI for compounds **5e** and **6**.

Table 4*:* Results of caspase-3 activation for compounds **5e** and **6**.

Table 5: Results of *in vitro* cyclin dependent kinase 2 inhibition (IC_{50} determination) for compound **6.**

Table 6: Results of P21 and P27 expression for compound **6**.

Scheme 1. Synthesis of compounds **1-7.**

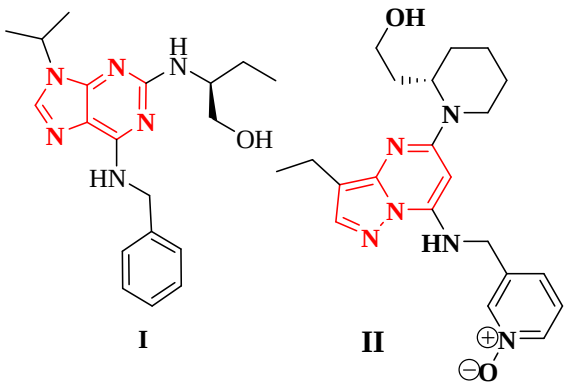

Figure 1: Chemical structure of some CDK2 inhibitors.

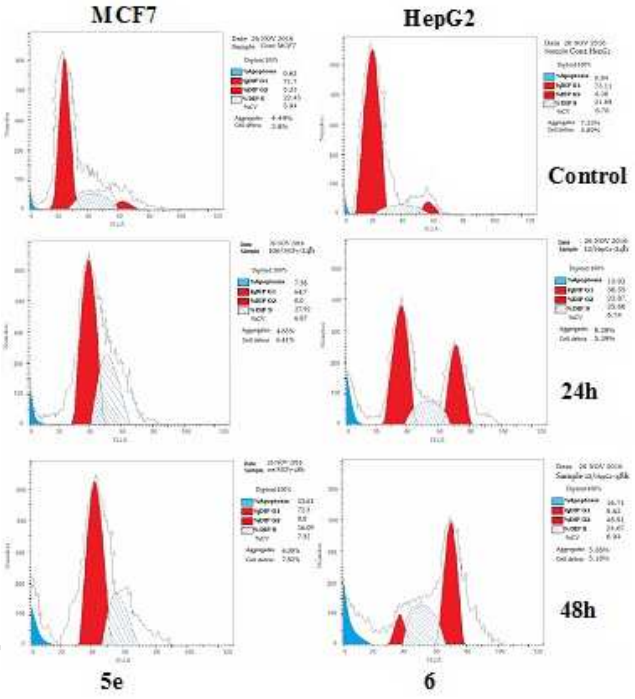

Figure 2: Cell cycle analysis of compound **5e** and **6** on MCF-7 and HepG2, respectively.

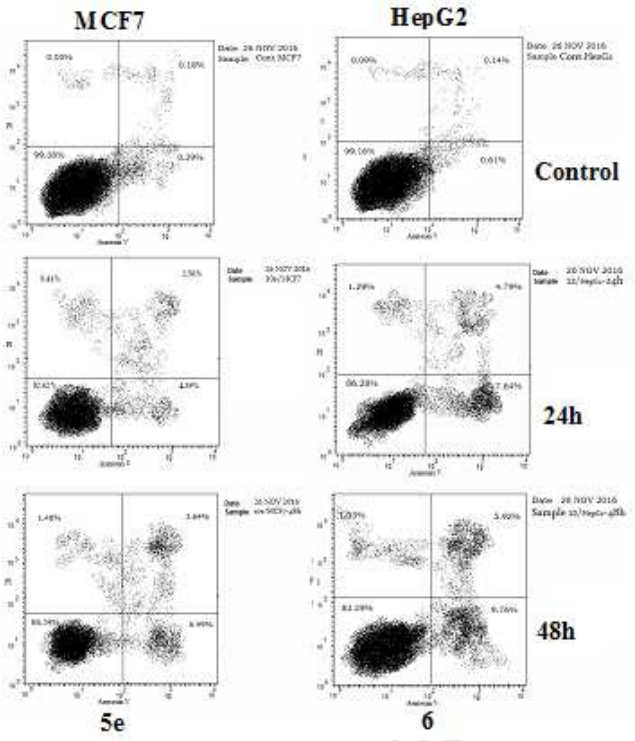

Figure 3: Apoptosis induction analysis using Annexin V/PI of compound **5e** and **6** on MCF-7 and HepG2, respectively.

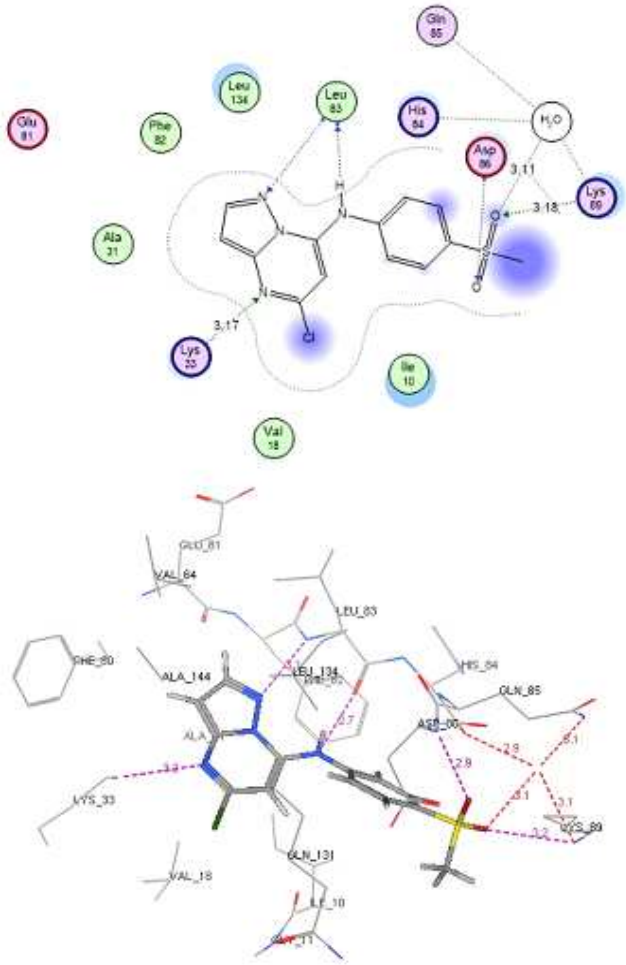

Figure 4: 2D (above) and 3D (below) interaction of ligand CT7 on the active site of CDK2.

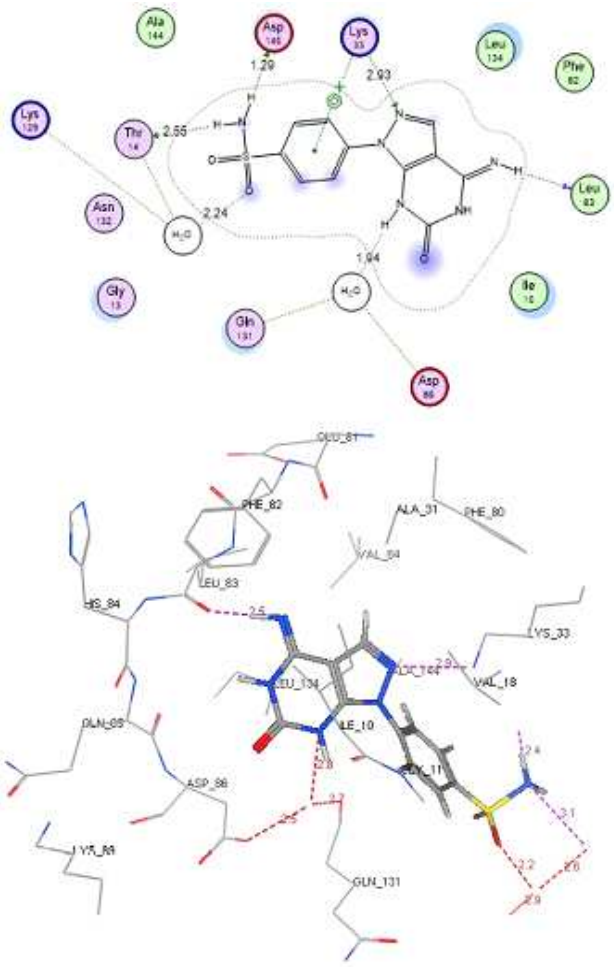

Figure 5: 2D (above) and 3D (below) interaction of compound **6** on the active site of CDK2.

Table 6: *In vitro* cytotoxic activity (IC_{50} µM) of compounds **3-7** against breast cancer cell line (MCF-7) and liver cancer cell line (HepG2).

Compounds	IC_{50} µM Breast cancer cell line (MCF-7)	IC_{50} µM Liver cancer cell line (HepG2)
3	>100	>100
4	>100	>100
5a	>100	77.60
5b	38.00	2.66
5c	2.50	23.90
5d	14.46	42.60
5e	1.40	>100
5f	>100	>100
6	>100	0.40
7	40.70	95.50
DOX.	1.02	0.90

Table 7: Cell Cycle analysis results for compounds **5e** and **6**.

Cell line	Sample code	% G0-G1	%S	%G2-M	%Apoptosis
MCF-7	Control	71.70	22.45	5.23	0.62
	5e / 24h	64.70	27.92	0.00	7.38
	5e / 48h	72.30	16.09	0.00	11.61
HepG2	Control	73.11	21.69	4.36	0.84
	6 / 24h	36.55	25.66	23.78	13.92
	6 / 48h	9.62	24.67	48.91	16.71

Table 8: Apoptosis induction analysis using Annexin V/PI for compounds **5e** and **6**.

Cell line	Sample code	% Early apoptosis	% Late apoptosis
MCF-7	Control	0.39	0.18
	5e / 24h	4.39	2.58
	5e / 48h	6.49	3.64
HepG2	Control	0.61	0.14
	6 / 24h	7.64	4.79
	6 / 48h	9.76	5.92

Table 9*:* Results of caspase-3 activation for compounds **5e** and **6**.

Cell line	Sample code	Conc. µM	Caspase-3 conc. (Pg/ml)
MCF-7	Control		13.9
	5e	1.40	440.9
HepG2	Control		17.2
	6	0.4	615.4

Table 10: Results of *in vitro* cyclin dependent kinase 2 inhibition (IC_{50} determination) for compound **6.**

Assay conc. µM	0.004	0.02	0.1	0.4	0.5
% Inhibition	12.591523	39.032691	53.129834	68.79842	81.808807

Table 6: Results of P21 and P27 expression for compound **6**.

	Sample code	Assay conc. µM	Residual conc. Pg/mL	% Activation
P21	Control		228.6	0.00
	6	0.40	251.6	10.06
P27	Control		316.6	0.00
	6	0.40	343.5	8.5

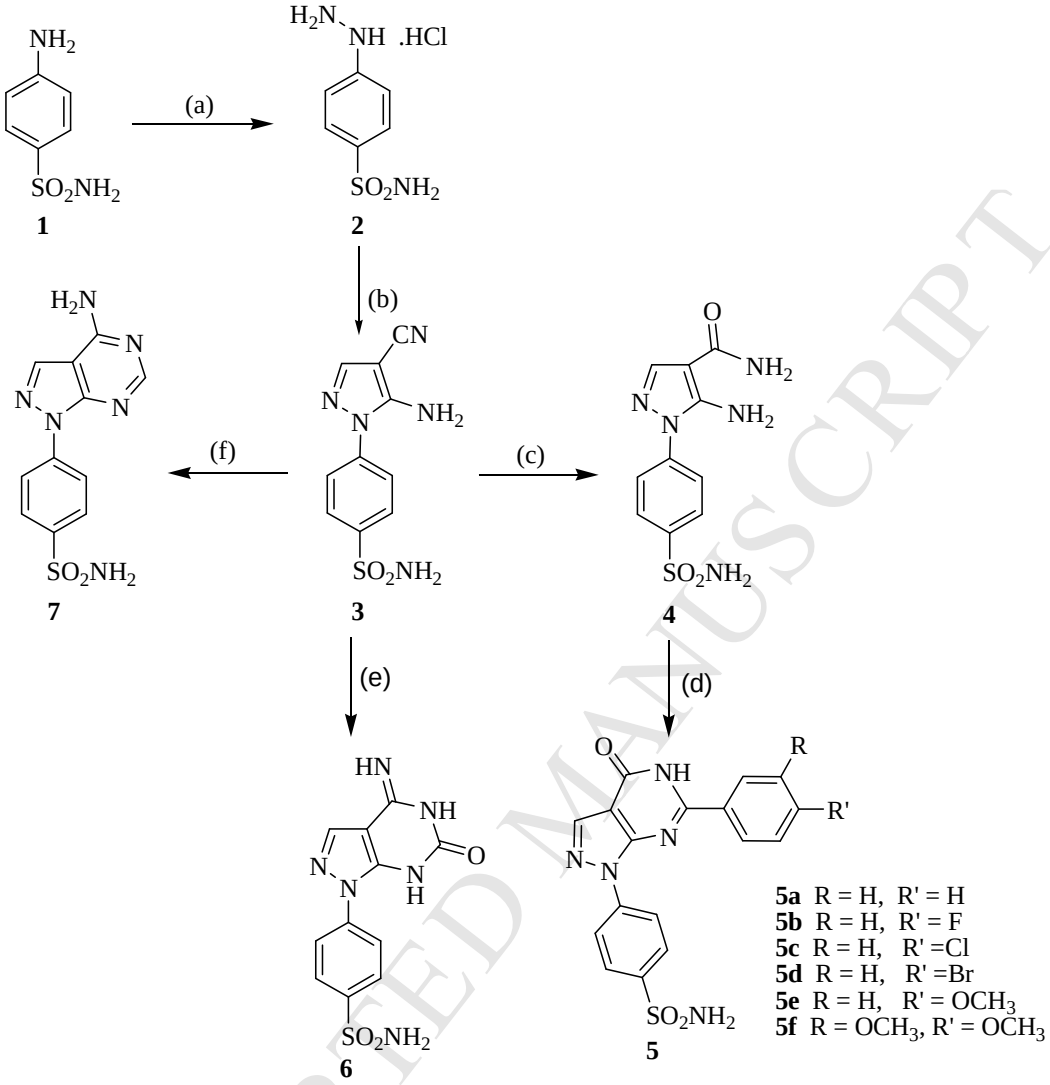

Scheme 1. Synthesis of compounds **1-7**

Reagents and conditions: (a) i- $NaNO_2$, HCl, 5 ^oC; ii- Na_2SO_3, HCl; (b) Ethoxy methylene malononitrile, anhyd. sodium acetate, absolute ethanol, reflux, 8h; (c) H_2SO_4, stir at room temperature, 16 h; (d) i- Aromatic aldehyde, DMF, 80 ^oC, 12-16 h; ii- 5% $Na_2S_2O_3$; (e) Urea, fusion, 20 min.; (f) Formamide, reflux, 16 h.

- Novel pyrazolo[3,4-d]pyrimidin-1-yl)benzenesulfonamide derivatives.
- *In vitro* cytotoxic activity on MCF-7 and HepG2 cell lines.
- *In vitro* activation of Caspase-3 and cell cycle analysis.
- *In vitro* inhibition of CDK-2 and molecular docking.